Proceedings of Global Power and Propulsion Society
ISSN-Nr: 2504-4400
GPPS Xi'an21
18th–20th October, 2021

www.gpps.global

GPPS-TC-2021-0102

Effectiveness of Active Flow Control Techniques in an Advanced S-Shaped Engine Intake

Philipp Max
Institute of Jet Propulsion
Bundeswehr University Munich
philipp.max@unibw.de
Neubiberg, Germany

Marcel Stößel
Institute of Jet Propulsion
Bundeswehr University Munich
m.stoessel@unibw.de
Neubiberg, Germany

Michael Krummenauer
Bundeswehr Technical Centre for
Aircraft and Aeronautical Equipment
michaelkrummenauer@bundeswehr.org
Manching, Germany

Reinhard Niehuis
Institute of Jet Propulsion
Bundeswehr University Munich
reinhard.niehuis@unibw.de
Neubiberg, Germany

ABSTRACT

The development of modern military aircraft has to meet considerable requirements in terms of reducing the system weight, installation space, as well as radar signature. For fighter aircraft, serpentine intakes are commonly used since they reduce the radar visibility of the engine, the system weight, and allow the optimal use of the installation space. However, these intake systems cause flow disturbances for the engine. To avoid penalties in engine performance, active flow control methods can be implemented for controlling the flow through the intake. The experiments undertaken at the Institute of Jet Propulsion (ISA) at the Bundeswehr University Munich used a scaled model of a compact double s-shaped intake duct with flow control techniques utilizing air injection and suction for boundary layer control and separation suppression. Detailed total pressure measurements with a Kiel probe rake at the exit plane of the duct show the effectiveness of the individual flow control mechanisms. Suction is applied at three different locations. For each configuration, the suction port diameter and mass flow rate are varied. For tests with injection, air is blown into the intake duct through a Coanda nozzle at two specific positions. The Coanda nozzle slot width and the number of slots were varied. The results demonstrate which parameters must be set to effectively influence the flow and achieve favorable distortion parameters at the intake duct's outlet.

INTRODUCTION

The major tasks of an aircraft engine intake are to provide the necessary air mass inflow for thrust generation, as well as a uniform flow with the required Mach number level at the compressor inlet plane with lowest possible losses. Especially for military aircraft, there are additional requirements such as a reduction of the radar signature (Wong et al., 2006), the reduction of the installation space and thus the system weight, as well as low sensitivity to high angles of attack. This can be achieved, among other things, by so-called serpentine ducts (S-duct) or double S-duct engine intakes. These engine intakes have no or a very limited direct line of sight through the intake onto the compressor stage. With these highly bend engine intakes a large reduction in radar cross section (RCS) can be realized by hiding the engine fan face as a radar return source (Rabe, 2003; Rao and Mahulikar, 2002).

Due to these contradictory requirements, the design of such an intake is a real challenge. On the one hand, the aim is to achieve low radar visibility, especially for Unmanned Aerial Vehicles (UAVs), by integrating the engine into the aircraft fuselage with an S-duct. On the other hand, the effect of the curvature of the S-duct centreline leads to cross-flow centrifugal pressure gradients which cause the boundary layer fluid to move in the direction of the pressure gradient thus inducing cross flows perpendicular to the main flow. Such secondary flows create an undesirable non-uniform total pressure distribution on the engine compressor face and may have many unfavorable influence on the engine's performance (Guo and Seddon, 1983). Hawthorne (1951) and Squire and Winter (1951) derived a formula for the inviscid case that relates the magnitude of the vorticity generated at an cascade in the direction of flow as a function of the intake cross vorticity and the total deflection angle. Bansod and Bradshaw (1972) demonstrated in an experimental study with several S-duct geometries that the generation of secondary flow is an inviscid phenomenon conditional on the presence of a velocity gradient, such as a boundary layer, at the inlet. Guo and Seddon (1983) have found that the swirl generated in an S-duct depends on the pressure gradients associated with the bends, the pressure gradients associated with the incidence of the inflow, the inertia of the flow, the viscous flow condition, especially the

presence of flow separation and the geometry of the duct's cross-sections. Furthermore, Guo and Seddon (1983) demonstrated that the resulting vortices cause an area of high total pressure loss at the duct outlet plane (DOP). The net effect of the secondary flow and the unfavorable pressure gradient of the diffuser result in an increased possibility of local boundary layer separation and thus an overall pressure loss at the duct outlet.

For this reason, various methods are used to reduce total pressure loss and suppress flow separation. In open literature, there are several publications concerning passive or active flow control techniques in S-ducts to reduce total pressure loss. These techniques are essentially classified into passive measures, which do not consume any additional energy, and active measures, which do require additional energy (Gad-el Hak, 1996). Methods including applications that involve suction and injection as well as vortex-generating jets belong to the active measures, and vortex generators or rough surfaces to the passive ones. For passive flow control mostly vortex generators are used. The purpose of vortex generators is to generate vortices that draw energy-rich fluid from the freestream into the slow-moving boundary layer to re-energize it (Anabtawi et al., 1999). In some studies, vortex generators are also used to redirect the boundary layer flow in the opposite direction to the naturally generated secondary flow, thus counteracting it (Reichert and Wendt, 1994, 1996). Studies show that both methods are successful, but the vortex generator orientation and location are only effective for certain flow conditions. Furthermore, vortex generators generate additional drag when not needed. This leads to active flow stabilizing measures that can be switched off when they are not required. The active methods treat the low momentum boundary layer which tends to separate. While the approach of boundary layer suction is to remove low-momentum fluid from the boundary layer, the blowing attempt is to re-energize low-momentum fluid. This should enable the boundary layer to withstand higher adverse pressure gradients without separation. Keerthi et al. (2017) have investigated suction to an S-duct at various positions and have shown that good values for the distortion parameters are obtained when suction is applied between 4% - 5% inlet mass flow. Debiasi et al. (2008) examined a moderate S-duct at different inlet Mach numbers and combined suction and blowing. With 2% recirculating mass flow, they obtained improved total pressure distributions at the aerodynamic interface plane (AIP). Ball (1985) performed tests on a high offset diffuser by using a porous wall to remove the low momentum fluid, similar to laminar flow control applications. Total pressure recovery was very high at about 2.3%, increasing the suction flow rate up to 4.7% caused a negligible improvement.

Most engine intakes in open literature on which flow stabilization measures have been investigated have solely round cross-sections and a smooth s-bend. However, literature in which more complex intake systems have been studied is very limited. Therefore, the military engine intake research duct (MEIRD) was developed at the Institute of Jet Propulsion (Rademakers et al., 2016). It is a short intake with a double s-bend, that changes its cross-section from kidney-shaped at the inlet to rectangular to circular at the DOP. This intake was developed as a pure research intake to investigate, among other aspects, measures to prevent flow separation within the duct. Due to its aggressive contour, certain flow control techniques that have worked well with simpler intake geometries may only have a minor effect on flow disturbances in case of the MEIRD. The work presented in this paper reports on active flow control measures like suction and blowing. These techniques have been implemented and evaluated utilizing a geometrical scaled MEIRD (MiniMEIRD). The results in this report show that a significant improvement in distortion parameters can be achieved by properly designed configurations. However, the location of the individual measures, the mass flow rate, and the respective suction or blowing area play an important role in the effectiveness of the flow control scheme.

EXPERIMENTAL SETUP

The experiments were performed on the scaled engine test facility (SETF) (Fig. 1), which is a 1:7,6 scaled model of the ISA's engine test facility (Bindl et al., 2009). The SETF was built to perform a large variety of experimental studies in a time and cost effective manner. The flow path in the SETF first passes over so-called inlet vanes at the top of the test bench (Fig. 1(a), A). The air then enters the highly curved engine intake (MiniMEIRD) (Fig. 1(a), B), passes the measuring rake (Fig. 1(a), C), the electric-starter shroud (Fig. 1(a), D), the engine (Fig. 1(a), E) and finally the mixing tube. During all experiments, the engine was kept at a constant speed. At this rotational speed, an inlet Mach number of 0,37 is achieved. This corresponds to a Reynolds number of $5 \cdot 10^5$ based on the diameter of the duct outlet plane (DOP).

In Fig. 1(b) the required peripheral apparatus is shown in form of a block diagram. In this test setup, either blowing or suction can be applied. In case of blowing, high pressure air is provided by an external system, including high resolution Coriolis flowmeter and flow control valves (cf. Fig. 1(b)). The mass flow was increased from 1% to 3.5% in 0.5% steps relative to the inlet mass flow rate. Suction is achieved using a ejector pump, which is controlled and driven by the before mentioned high pressure air system. The supply pressure for the ejector pump has been kept constant throughout all tests. The suction mass flow was 0.25%, 0.6%, 1% and was increased further from 1% in 0.5% steps up to a maximum of 6.5%. However, 6.5% was not achieved in all investigated configurations due to very small suction holes and the associated increase in pressure loss in some of the tested configurations.

The MiniMEIRD investigated in the SETF is a 1:7,6 scale model of the MEIRD (Rademakers et al., 2016). The centerline is determined by four cross-sections and shown in red in Fig. 1(b). The intake-outlet diameter (D_{DOP}) is 60 *mm*. The cross-sections are positioned along the centerline in their centers of area. The cross-section (CS_0) (cf. Fig. 1(b)) at the inlet represents a kidney shape which changes via the cross-section at 40% centerline-length (CS_{40}) to a rectangular shape at the cross-section at 72% (CS_{72}) centerline-length. At the DOP, the cross-section is a circular profile. A surface has been overlaid on these cross-sections, which result in the MEIRD geometry. The intake investigated has a length in the x-direction of $3 \cdot D_{DOP}$ and a diffusion factor of $A_{DOP}/A_{DIP} = 1.17$. Furthermore, the geometry is symmetric to the xz-plane of the duct (cf. Fig. 1(b)). The MiniMEIRD does not provide a direct line of sight from the duct inlet plane (DIP) to the DOP at any angle of attack, thus reducing the radar signature

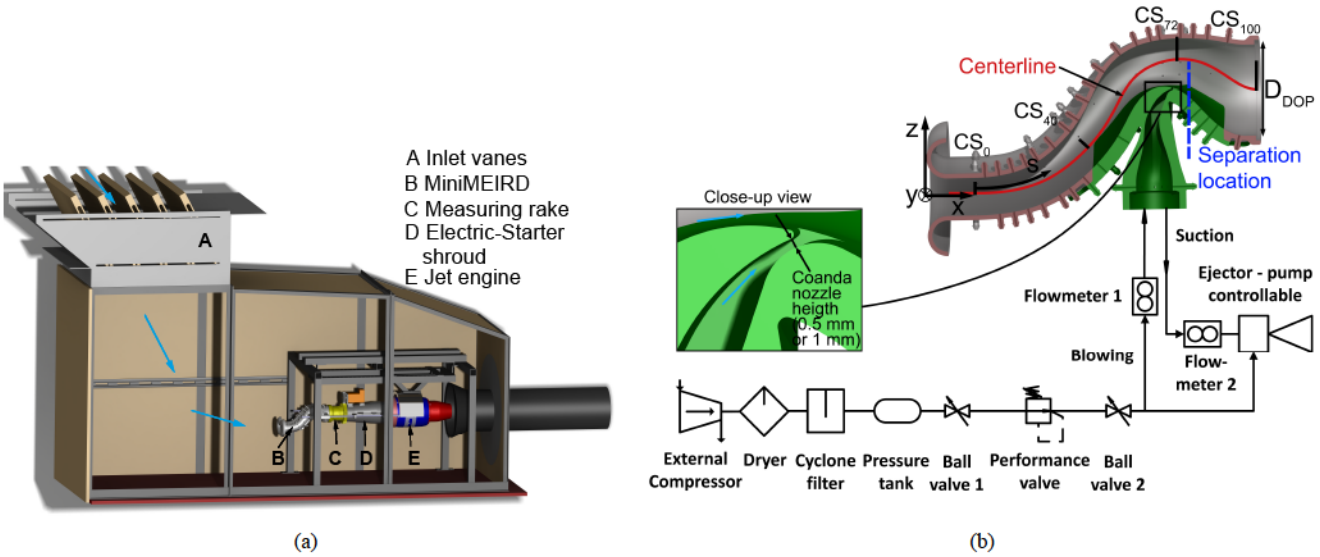

Fig. 1 (a) Schematic overview of the scaled engine test facility (SETF) at the ISA (front side walls not shown for a better overview), (b) Block diagram of the experimental setup (inlet is shown as cut-away view); Duct centerline: red line; Green blowing insert as cut-away view; Separation location: blue line; Detail view of the Coanda nozzle

of the compressor to a maximum. As numerical studies of this intake have already shown, the flow separates between $x_{rel} = 0.75$ to $x_{rel} = 0.88$ as intended (Haug et al., 2018). To actively manipulate the flow in this zone, the intake has a cutout at this location (Fig. 1(b) green insert). Different configurations of suction or blowing inserts can be installed in this cutout. A sample of the inserts is shown in Fig. 2. The blue dashed line represents the separation location. The specific inserts are depicted in green and the blowing and suction ports are marked in orange. For better visibility of the inserts, the intake is shown as a 1/4-cutaway view. The inserts are mounted to the inlet with four screws. All inserts are symmetrical to the xz-plane. The injection is performed via a Coanda nozzle for all blowing inserts. The following geometrical parameters were varied:

- The Coanda slot height (0.5 *mm* or 1 *mm*) and thus the area over which the air is blown in (Fig. 1(b))
- The x-position of the injection (compare Fig. 2(d) and (e))
- The number of slots, whereby the slot in the symmetry plane is always present (Fig. 2 (e))
  - If there are several injection slots, the y-distance of the outermost slots to the slot in the symmetry plane. (While the slot width in y-direction is always 10 *mm*)
  - The angle of the outer slots (Fig. 2 (f))

To distinguish the different inserts and the set parameters there is a uniform nomenclature. As an example, the Blo_3/30/0.75/25/60° insert is explained (Fig. 2(f)). The abbreviation "Blo" stands for a blowing insert with three slots and a total blowing area of 30 mm^2. The Coanda nozzle is located at $x_{rel} = 0.75$. The center of the outer slots is placed at the y-position 25 *mm* and due to the symmetry of the insert at −25 *mm*. If there are several slots, the slot width is always 10 *mm* and as already mentioned the slot in the symmetry plane is always present. If the outer slots are angled, the corresponding angle still follows in the nomenclature. In this example 60°. For the blowing configurations with only one slot, the 4th number indicates the end of the slot width in the y-direction (Fig. 2(d)).

All suction inserts consist of a perforated plate with 60 holes perpendicular to the inner wall of the duct. For the suction configurations, the diameter of the suction holes (1 *mm*, 1.5 *mm*, 2 *mm* and 3 *mm*) and the position of the perforated plate in the x-direction were varied (Fig. 2(a), (b), (c)). There is also a uniform identifier for the suction insert configurations, which is explained using insert Sc_3/0.68_0.81 as an example (Fig. 2(b)). The abbreviation "Sc" indicates a suction configuration. This configuration has suction holes diameter of 3 *mm*. The first row of suction holes in flow direction is located at $x_{rel} = 0.68$ and the last row at $x_{rel} = 0.81$. The suction holes were spaced equidistantly along the lower wall centerline and there were no different suction hole diameters within one configuration.

The performance of each configuration was evaluated using the distortion parameters as defined in the SAE ARP 1420C standard (Turbine Engine Inlet Flow Distortion Committee, 2017). For this purpose, the total pressure distribution in the AIP was measured with a Kiel probe rake (Max et al., 2020). The circumferential distortion intensity (CDI) at the *k*th radial location ("ring") is defined as

$$CDI_k = max_k \left(\frac{P_{t,AV} - P_{t,AV-LOW}}{P_{t,AV}} \right), \tag{1}$$

where $P_{t,AV}$ is the ring averaged total pressure and $P_{t,AV-LOW}$ is the subset of only those values that are lower than $P_{t,AV}$ ($P_{t,AV-LOW} < P_{t,AV}$). The maximum of k rings indicates the highest circumferential distortion intensity. The circumferential distortion extent (CDE) is equal to the angular extent over which the $P_{t,AV-LOW}$ values lie. The radial distortion intensity (RDI) defined at a given

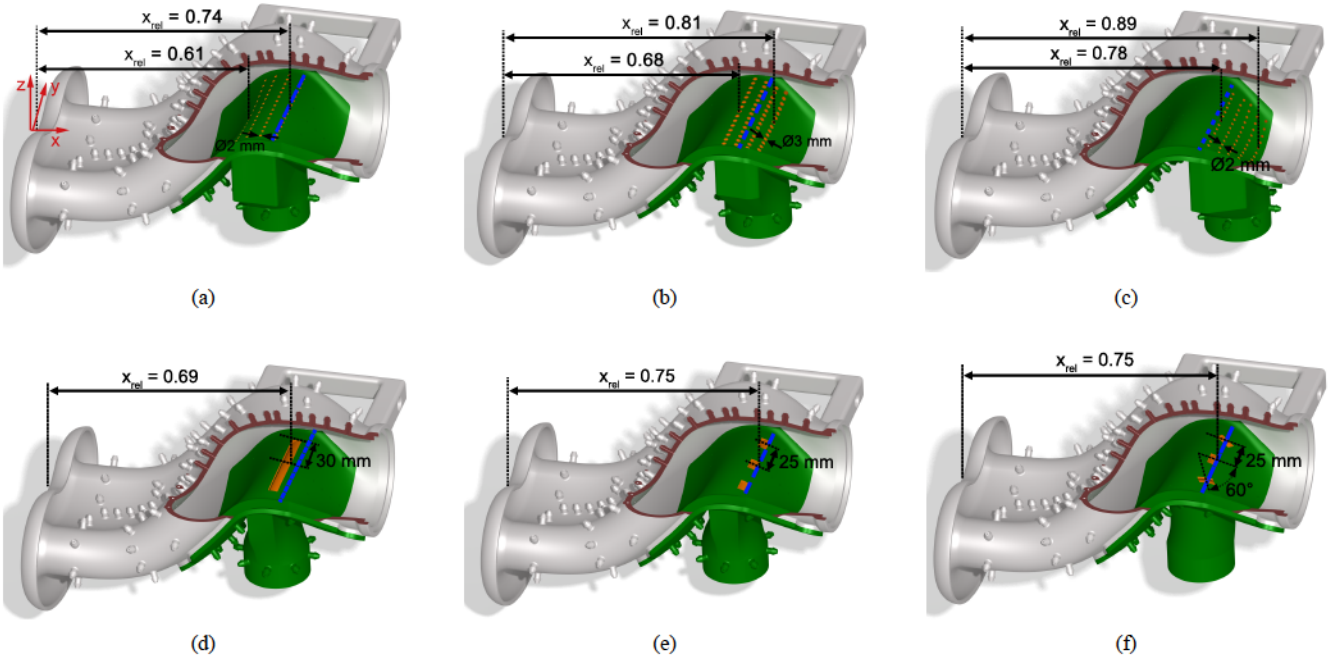

Fig. 2 Examples of suction and blowing insert configurations, (a) suction configuration Sc_2/0.61_0.74, (b) suction configuration Sc_3/0.68_0.81, (c) suction configuration Sc_2/0.78_0.89, (d) blowing configuration Blo_1/60/0.69/30, (e) Blo_3/30/0.75/25, (f) Blo_3/30/0.75/25/60°

radius is calculated as the ratio of the difference between the face total pressure ($P_{t,FAV}$) and the ring average total pressure $P_{t,AV}$ to the face average total pressure:

$$RDI_k = max_k \left(\frac{P_{t,FAV} - P_{t,AV_k}}{P_{t,FAV}} \right) \tag{2}$$

The RDI values can be both positive and negative. Where positive RDI values mean that the ring average total pressure $P_{t,AV}$ is lower than the face average total pressure $P_{t,FAV}$ and vice versa. A further well known distortion coefficient is the DC60 parameter:

$$DC60 = max_{60°} \left(\frac{P_{t,FAV} - P_{t,Worst-60°}}{P_{t,FAV} - p_{AV}} \right), \tag{3}$$

where $P_{t,FAV}$ is the face average total pressure as described at the RDI. $P_{t,Worst-60°}$ is the mean of the measurement points in a sector of 60° with the lowest total pressure values. And p_{AV} is the average static pressure in the AIP. The DC60 distortion coefficient was first defined by Reid (1969). Another parameter, which gives a first impression of the performance of an intake system, is the pressure recovery

$$PR = \left(1 - \frac{P_{t,AV-DOP}}{P_{t,amb}} \right) \cdot 100\% = \left(1 - \frac{P_{t,FAV}}{P_{t,amb}} \right) \cdot 100\%, \tag{4}$$

where $P_{t,amb}$ is the average total ambient pressure in the test facility. A more detailed description of these parameters can be found in (Turbine Engine Inlet Flow Distortion Committee, 2017).

RESULTS AND DISCUSSION

Baseline Duct

First, the intake without flow stabilizing measures was investigated. This baseline case serves on the one hand for the flow characterization of the intake and on the other hand as a reference to evaluate and assess the efficiency of the active flow control measures. For this reason, the total pressures in the AIP and the static wall pressures at the upper wall centerline (red) and lower wall centerline in the symmetry plane (grey) of the inlet were recorded (Fig. 3). The relative static wall pressures of the upper and lower wall centerline, as well as the contour of the duct in its symmetry plane, are shown in Fig. 3(a). The relative pressures are always the respective measured pressure to the ambient pressure and the relative x- and z-axis are normalized with the total length of the inlet. The wall pressure distribution of the lower wall centerline (grey dashed line) can be described to a certain extent by the curvature path of the duct wall. Up to $x_{rel} = 0.3$, a small increase in pressure can be seen. Due to the centrifugal force, the air is pushed in the direction of the lower wall, which leads to this pressure rise. Besides, the cross-sectional area orthogonal to the centerline increases steadily in a linear way up to $x_{rel} = 0.7$ (corresponds to $S = 0.72\%$) (Rademakers

et al., 2016). The wall curvature also initially tends toward the flow, which corresponds to an adverse pressure gradient and thus leads to a flow deceleration. Between $x_{rel} = 0.53$ and $x_{rel} = 0.63$, the curvature diminishes (positive pressure gradient) and the flow accelerates strongly, which is indicated by the pressure drop. The pressure increases again from $x_{rel} = 0.63$ until between $x_{rel} = 0.7$ and $x_{rel} = 0.8$ a pressure plateau is present. As the CFD simulations by Haug et al. (2018) show, this pressure plateau can be attributed to flow separation. The wall pressure curve on the upper wall centerline also exhibits a pressure increase for $0.4 \leq x_{rel} \leq 0.6$. Downstream of $x_{rel} = 0.6$, the flow accelerates as can be observed from the pressure drop. Based on this analysis and the numerical investigations, the possible x-positions for the suction and injection configurations are obtained. The areas of the x-positions over which the respective suction configuration passes are shown as a hatched area under the relative static wall pressure profile of the lower wall centerline (Fig. 3(a)). The green shaded area represents all suction configurations whose first row of holes starts at $x_{rel} = 0.61$ and ends at $x_{rel} = 0.74$ (Sc_#/0.61_0.74). The orange shaded area indicates the range of suction configurations that start with a row of holes at $x_{rel} = 0.68$ and have the last one at $x_{rel} = 0.81$ (Sc_#/0.68_0.81). All suction configurations that go from $x_{rel} = 0.78$ to $x_{rel} = 0.89$ are marked with the purple shaded area (Sc_#/0.78_0.89). The blowing position $x_{rel} = 0.69$ is shown as a black vertical line. The second injection position in the x-direction is identical to the separation location ($x_{rel} = 0.75$), which is shown as a vertical blue dashed line.

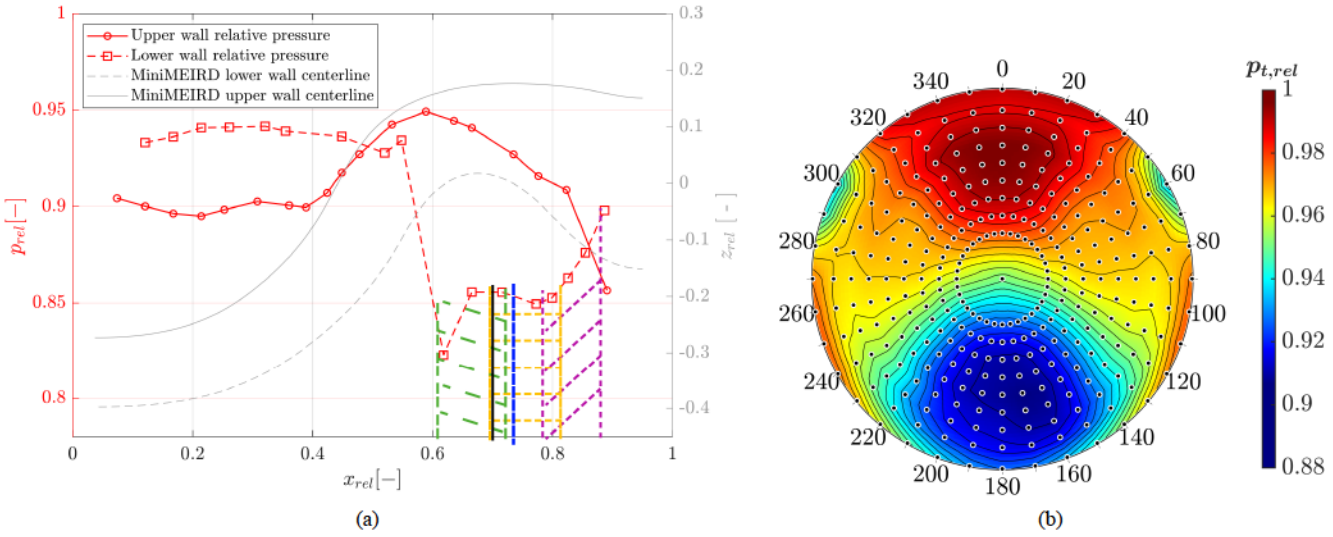

Fig. 3 (a) Static wall pressure plot, with the positions of the blowing and suction configurations, as well as the separation location line, (b) Baseline AIP plot with measurement points

In the AIP plot the measuring points are marked by black dots with a white frame (Fig. 3(b)). In total, the AIP was resolved with 325 measuring points, from which the distortion parameters were calculated as well. The AIP plot in Fig. 3(b) depicts an immense total pressure disturbance in the lower part of the intake-outlet. According to the numerical investigations by Haug et al. (2018), this total pressure disturbance is mainly caused by the separation bubble. The total pressure plot also shows that the flow in the upper part nearly reaches the ambient pressure. At 60° and 300° at the wall, two small total pressure disturbances show up. According to (Haug et al., 2018), these smaller total pressure disturbances are caused each by a vortex pair, which is generated by secondary flow effects in the first bend of the MiniMEIRD. The baseline configuration has a DC60 distortion parameter of 0.45, which is too high for most modern aircraft engines to operate stable. The CDI is found to be 0.0334 and the CDE is 163°, while the minimum RDI is −0.00922 and the maximum RDI is 0.05696 (Fig. 4).

Duct performance with active flow control

Fig. 4 depicts the analyzed distortion parameters in the form of a bar chart. The primary y-axis shows the individual distortion parameter values and the x-axis identifies the particular blowing or suction configuration. On the secondary y-axis, the suction or blowing mass flow rate of the respective configuration is plotted. Whereas the full name of the inserts is only shown in the DC60 diagram but can be transferred vertically to the diagram above. Configuration no. 1 corresponds to the baseline configuration and no. 2 to insert *Blo*_1/60/0.69/30, and so on. An efficient configuration has low distortion parameters and at the same time a low mass flow rate to achieve those. Those configurations are reflected by a low column height of the distortion parameters and the mass flow rate. To better classify the relative x-position of the suction and blowing configurations, these were marked with the same colors as already shown at the wall pressure curve (cf. Fig. 3(a)).

Suction

In case of suction, the configurations with a suction hole diameter of 1.5 *mm* and 2 *mm* and a relative x-position of 0.68 to 0.81 or 0.61 to 0.74 show satisfactory performance in terms of low distortion parameters and, simultaneously, a low suction mass flow. With the configuration *Sc*_1.5/0.68_0.81 (no. 21), a DC60 value of 0.1 can be achieved with a suction mass flow rate of

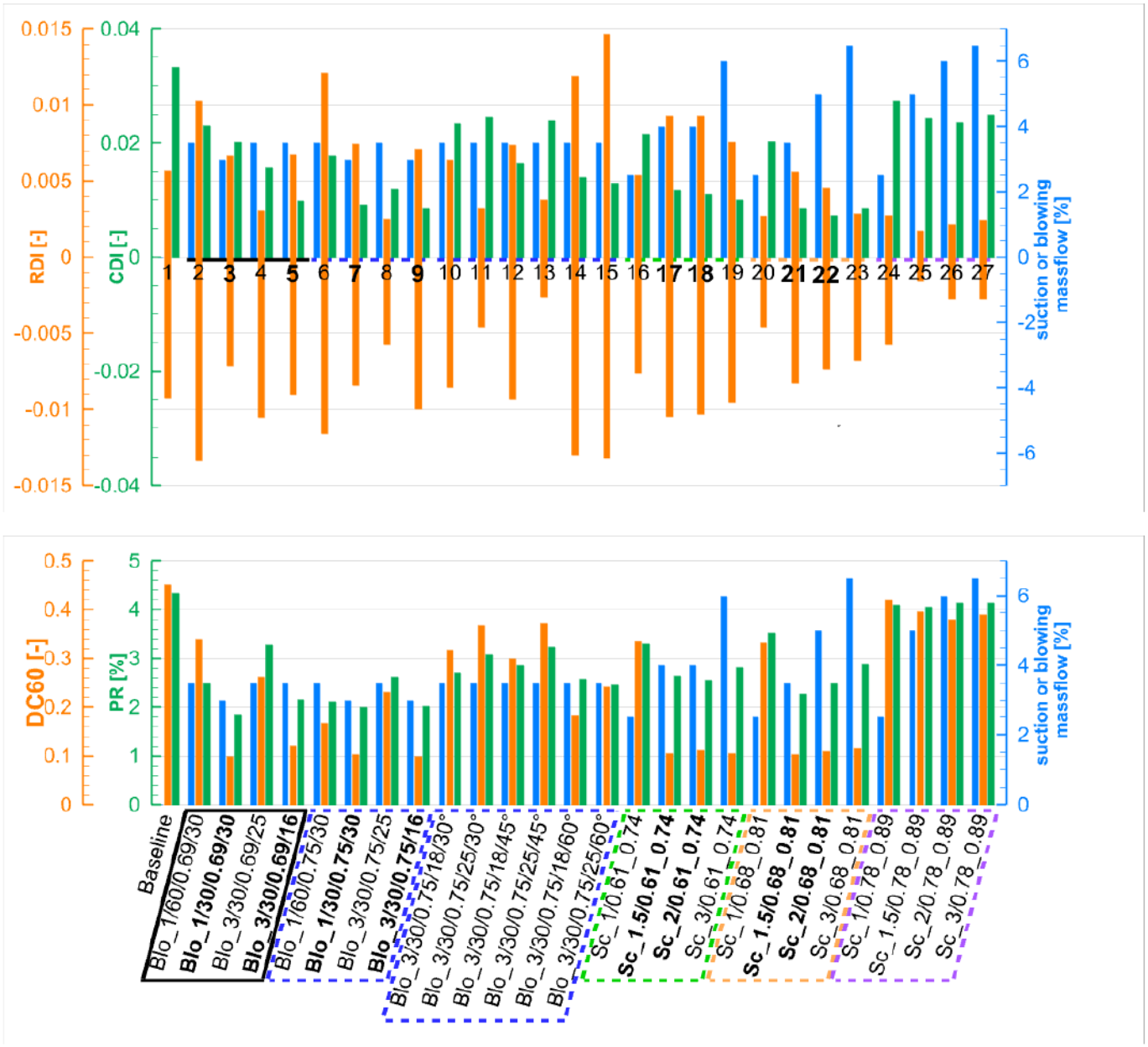

Fig. 4 Distortion parameters and the respective suction or blowing mass flow rate

3.5%. The other parameters, such as a pressure recovery of 2.5% or a CDI of 0.0085, are also at a very low level compared to the baseline case. However, the RDI is only slightly affected compared with the baseline configuration. With the configurations *Sc*_1.5/0.61_0.74 (no. 17), *Sc*_2/0.61_0.74 (no. 18), and *Sc*_2/0.68_0.81 (no. 22), similarly low DC60 values between 0.1 and 0.11 are achieved, but with higher suction mass flow rate between 4% and 5%. The pressure recovery, as well as the CDI, are slightly higher than at the configuration *Sc*_1.5/0.68_0.81. However, for configurations *Sc*_1.5/0.61_0.74 (no. 17) and *Sc*_2/0.61_0.74 (no. 18) the RDI is worse compared to the values of the baseline configuration. Very low distortion parameter values can be achieved with a suction hole diameters of 3 *mm* (no. 19 and no. 23) but only with high suction mass flows between 6% and 6.5%. These high mass flow rates reduce the performance of the active flow control system significantly.

On the other side with a suction hole diameters of 1 *mm*, a maximum mass flow of 2.5% could be extracted, resulting in DC60 values of 0.33 to 0.42, which is a negligible small improvement compared to the baseline configuration. With 1 *mm* exhaust holes, the pressure loss through the holes is too high, and therefore the suction mass flow rate was limited to 2.5%. The configurations at $x_{rel} = 0.78$ to $x_{rel} = 0.89$ and thus removing the air after the separation line show the least influence on the distortion parameters except for the RDI. The DC60 values are between 0.42 and 0.39, only slightly lower than the one of the baseline configuration. The pressure recovery is 4.1% and the CDI ranges from 0.027 to 0.024. On the other hand, the RDI improves and is between 0.0028 and -0.0057, which are the lowest RDI values obtained of all configurations. Reid (1969) showed in a study that the circumferential total pressure distortion has a more severe impact on the surge margin than the radial variation although other researchers attribute significant importance to the RDI. The values of the suction configurations imply that suction should be applied before the detachment line and preferably with a hole diameter between 1.5 *mm* to 2 *mm* with a suction mass flow rate

between 3.5% and 5%.

The total pressure plot at the AIP of the configuration *Sc*_1.5/0.68_0.81 (Fig. 5(a)) shows, that with a suction mass flow rate of 3.5% the total pressure disturbance at 180° completely dissipates and the ambient pressure is almost reached. The total pressure disturbances at 60° and 300° are still present and even get more intensive compared to the baseline configuration. The total pressure plot is symmetrical and has an area of low total pressure at the outside boundary between 60° and 160°.

While the vertical center from 0° to 180° shows an area of higher total pressure. A similar situation is shown by the total pressure plot of the configuration *Sc*_1.5/0.61_0.74 and 4% suction mass flow (Fig. 5(b)). The total pressure disturbance at 180° was reduced. Nevertheless, there is a low total pressure area in a u-shape extending from 60° over 180° to 300° at the outer circumference. The AIP plot of the configuration *Sc*_1.5/0.78_0.84 (Fig. 5(c)) shows no significant change compared to the baseline configuration. This is also reflected in the distortion parameters except for the RDI values, which are negligibly below those of the baseline.

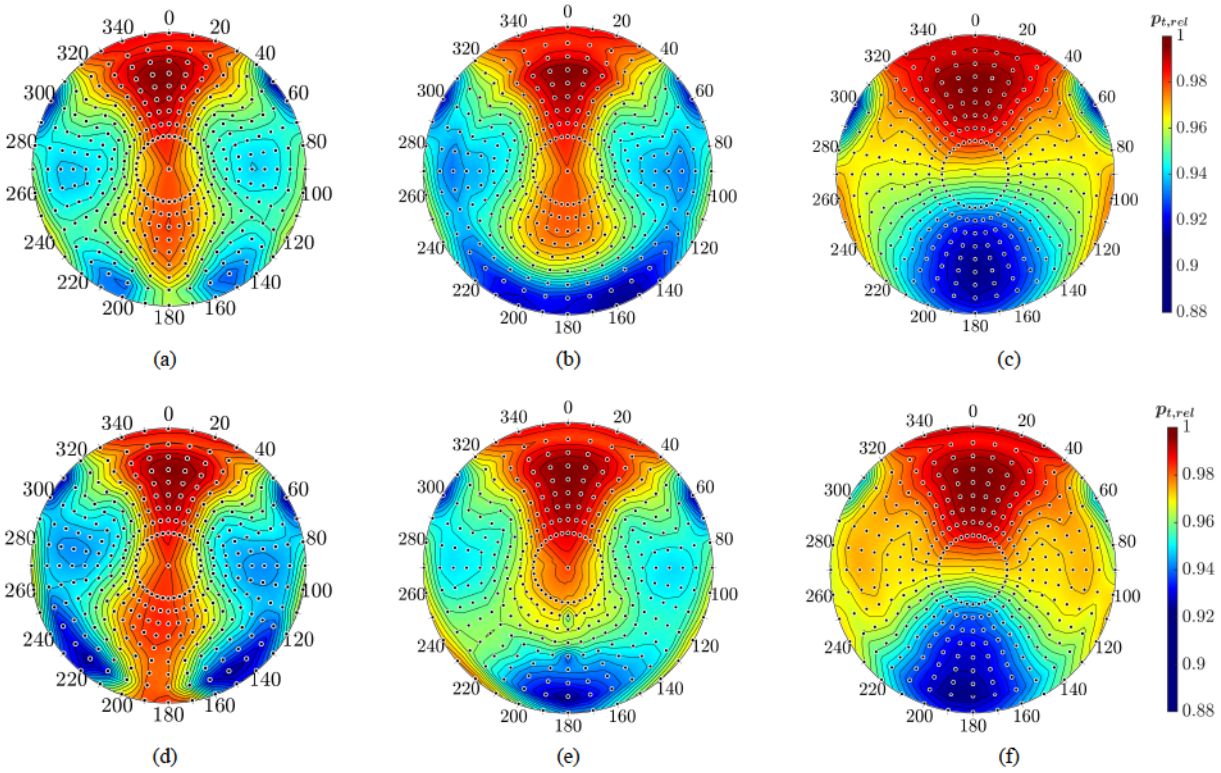

Fig. 5 AIP relative total pressure plots for suction and blowing configurations, (a) Configuration Sc_1.5/0.68_0.81 (no. 21) with 3.5% suction mass flow rate, (b) Configuration Sc_1.5/0.61_0.74 (no. 17) with 4% suction mass flow rate (c) Configuration Sc_1.5/0.78_0.89 (no.25) with 5% mass flow rate, (d) Configuration Blo_1/30/0.75/30 (no. 7) with 3% blowing mass flow rate, (e) Configuration Blo_3/30/0.69/16 (no. 5) with 3.5% blowing mass flow rate, (f) Configuration Blo_3/30/0.75/25/45° (no. 13) with 3.5% blowing mass flow rate

The results show that to obtain a proper performing suction configuration, the following design steps must be taken into account:

- The separation line must be identified as accurately as possible to be able to set the suction position.
- The suction holes position should be before or slightly downstream of the separation line. Positioning all suction holes downstream the separation line shows negligible improvement of the distortion parameters.
- For low distortion parameters, suction mass flow rate between 3.5% and 5% of the inlet mass flow is sufficient.
- The suction hole diameter can be estimated using the suction mass flow and the pressure loss over the suction hole.

Considering the above mentioned criteria the suction configurations (Sc_1.5/0.61_0.74 (no. 17), Sc_2/0.61_0.74 (no. 18), Sc_1.5/0.68_0.81 (no. 21) and Sc_2/0.68_0.81 (no. 22)) provide best performance in terms of low distortions parameters (cf. Fig. 4 marked bold).

Blowing

When blowing without obliquely positioned outer slots, the results show that with the position at $x_{rel} = 0.75$ directly at the detachment line, slightly lower distortion parameters can be achieved than with comparable configurations at the position $x_{rel} = 0.69$ (cf. Fig. 4). The *Blo*_1/60/0.69/30 (no. 2) and *Blo*_1/60/0.75/30 (no. 6) inserts differ only in their different relative x positions. With the *Blo*_1/60/0.75/30 insert, a DC60 value of 0.16 is achieved with an injection mass flow of 3%, while the insert at the position $x_{rel} = 0.69$ results in a DC60 value of 0.33 with the same injection mass flow. Thus the blowing position

$x_{rel} = 0.75$ is more effective. The same result is shown by the remaining distortion parameters, each with favorable values for the position $x_{rel} = 0.75$. Further comparisons of inserts, where the x_{rel} position was the only parameter varied, show the same trend as already described. Only the RDI parameter is lower for insert *Blo*_3/30/0.69/16 (no. 5) than for insert *Blo*_3/30/0.75/16 (no. 9). However exceptions are inserts *Blo*_1/30/0.69/30 (no. 3) and *Blo*_1/30/0.75/30 (no. 7), both achieve a DC60 of 0.1. In terms of pressure recovery and RDI, insert *Blo*_1/30/0.69/30 achieves lower values than insert *Blo*_1/30/0.75/30 for the same injection mass flow rate. With regards to the CDI, insert *Blo*_1/30/0.75/30 is better again with a value of 0.009 compared to 0.02. For the Coanda nozzle height and thus the injection area, the configurations with a Coanda nozzle height of 0.5 mm and thus an injection area of 30 mm^2 consistently perform better than the configurations with an injection area of 60 mm^2. Due to the smaller area, the air is injected at a higher velocity and thus a higher momentum is introduced, which energizes the detached boundary layer better. Another conclusion that can be derived is the positioning of the outer slots in configurations with three slots. It can be observed that the configurations with the outer slots closer to the middle slot generate lower values for the DC60, CDI, and PR. Only the RDI of configuration *Blo*_3/30/0.75/25 (no. 8) is better than *Blo*_3/30/0.75/16 (no. 9).

The AIP plot of the injection configuration *Blo*_1/30/0.75/30 (cf. Fig. 5(d)) shows a similar total pressure distribution as seen at the suction configuration *Sc*_1.5/0.6/0.68_0.81 (Fig. 5(a)). The AIP plot is separated into two parts at its center. In the middle, there is an area where the ambient pressure is reached. To the right and left of this two regions exist with lower total pressure. It can be supposed that these two regions of lower total pressure are created by the fact that the total pressure disturbance at 180° almost disappears. Because of this, the two total pressure disturbances at 30° and 300° get more space and enlarge. To control these two side regions as well, additional configurations with three slots were investigated in which the outermost slots are angled. As an example of these configurations, the *Blo*_3/30/0.75/25/45° insert is depicted (Fig. 5(f)). It is found that the area of total pressure disturbance becomes narrower due to the lateral angled slots. However, the total pressure distortion at 180° shows only a slight influence due to the slot being placed in the plane of symmetry. To influence the total pressure disturbance at 180° and thus achieve favorable performance parameters, the entire momentum applied to the inlet in the x-direction is required. This can also be seen in Fig. 5(e), where a configuration with 3 slots in the flow direction (without angled outer slots) is depicted. Here the total pressure disturbance at 180° is strongly influenced and lower distortion parameters are achieved, while the disturbances at 60° and 300° are nearly the same as in Fig. 5(d).

In order to obtain satisfactory blowing configurations, the following aspects should be considered:

- As already mentioned for suction, the separation line for positioning the blowing configuration must be known.
- The blowing position should be as close as possible to the separation line.
- The blowing mass flow rate should be in between 3% and 4% of the inlet mass flow.
- To introduce as much momentum as possible into the main flow, the slot height at the design point should be as close as possible to the choking limit. The slot hight can be estimated using the blowing mass flow rate and the pressure.
- In configurations with three slots, at least one slot should be in the middle (xz-plane cf. Fig. 2 (e)) and the other close to the middle. Angled outer slots (cf. Fig. 2 (f)) do not improve the distortion parameters or the total pressure disturbance in the AIP. In order to obtain a tangential injection and thus a high impact on the separation bubble, injection should be performed via a Coanda nozzle.

Consideration of above design lead to injection configurations (Blo_1/30/0.69/30 (no. 3), Blo_3/30/0.69/16 (no. 5), Blo_1/30/0.75/30 (no. 7), Blo_3/30/0.75/16 (no. 9) cf. Fig. 4 marked bold) featuring low distortion parameters.

CONCLUSIONS

The investigations were carried out on a double S-shaped engine intake which, due to its geometry, does not allow a direct line of sight to the fan and thus has very effective stealth characteristics but a strong curvature of the flow path. The performance losses resulting from the bent intake were presented at the baseline insert in the form of the distortion parameters (DC60 = 0.45, CDI = 0.0334). The experiments demonstrate when comparing the best performing configurations (cf. Fig. 4 bold marked configurations) in terms of the DC60 distortion parameter, DC60 values of 0.1 are achievable with both blowing and suction. This represents an improvement of 78% compared to the baseline case. However in order to achieve this minimal DC60 level an injection mass flow rate between 3% and 3.5% and a suction mass flow rate of 3.5% to 5% is necessary. This indicates a slight preference for injection over suction, but no conclusion can be drawn about the overall engine performance due to the external supply of the suction and injection mass flow. A comparison of the above mentioned configurations with regard to the CDI parameter shows that this is stronger reduced by suction than by injection. The CDI values for suction range between 0.0073 and 0.012, while those for injection range between 0.0086 and 0.02. No clear trend emerges for the RDI. Moreover, it is not always reduced compared to the baseline case. Furthermore, it was found that to reduce the total pressure disturbance at 180°, the slots should be placed close to the center plane. If the outer slots are angled, there is not enough momentum to control the total pressure disturbance at 180° and the distortion parameters are worse than in configurations with slots in the direction of flow. The results demonstrate that by providing the correct position and the appropriate mass flow, the separation bubble in the intake can be suppressed successfully, and thus the efficiency of the intake is improved significantly.

NOMENCLATURE

Abbreviations		Symbols	
AIP	Aerodynamic interface plane	S	Position at the centerline, percentage wise
DOP	Duct outlet plane	DC60	Distortion coefficient
DIP	Duct inlet plane	CDI	Circumferential distortion intensity
ISA	Institute of Jet Propulsion	RDI	Radial distortion intensity
MEIRD	Military Engine Intake Research Duct	x,y,z	Cartesian coordinates
MiniMEIRD	scaled model of the MEIRD	PR	Pressure recovery
RCS	Radar cross-section	$P_{t,AV}$	Average total pressure
S-duct	Serpentine duct	$P_{t,FAV}$	Average total pressure over all points in the AIP
SETF	Scaled engine test facility	$P_{t,AV-LOW}$	Average total pressure over points whose values are less than that of the ring average
UAVs	Unmanned Aerial Vehicles	$P_{t,amb}$	Ambient pressure
CS_0	Cross section at S = 0%	$P_{t,Worst-60°}$	Mean total pressure measurement points in a sector of 60° with lowest total pressure values
CS_{40}	Cross section at $S = 40\%$		
CS_{72}	Cross section at $S = 72\%$		
CS_{100}	Cross section at $S = 100\%$	x_{rel}	relative x coordinate

REFERENCES

Anabtawi, A., Blackwelder, R., Lissaman, P. and Liebeck, R. (1999), An experimental study of vortex generators in boundary layer ingesting diffusers with a centerline offset, *in* '35th Joint Propulsion Conference and Exhibit', American Institute of Aeronautics and Astronautics, Reston, Virigina.
URL: *https://doi.org/10.2514/6.1999-2110*

Ball, W. H. (1985), 'Tests of wall suction and blowing in highly offset diffusers', *Journal of Aircraft* **22**(3), 161–167.
URL: *https://doi.org/10.2514/3.45102*

Bansod, P. and Bradshaw, P. (1972), 'The flow in s-shaped ducts', *The Aeronautical Quarterly* **23**(2), 131–140.
URL: *https://doi.org/10.1017/S0001925900006004*

Bindl, S., Muth, B. and Niehuis, R. (2009), Experimental investigations on macro-aerodynamics within a jet engine ground test facility, *in* '45th AIAA/ASME/SAE/ASEE Joint Propulsion Conference & Exhibit', p. 4828.
URL: *https://doi.org/10.2514/6.2009-4828*

Debiasi, M., Herberg, M., Zeng, Y., Tsai, H. M. and Dhanabalan, S. (2008), Control of flow separation in s-ducts via flow injection and suction, *in* '46th AIAA Aerospace Sciences Meeting and Exhibit', American Institute of Aeronautics and Astronautics, Reston, Virigina.
URL: *https://doi.org/10.2514/6.2008-74*

Gad-el Hak, M. (1996), 'Modern developments in flow control', *Applied Mechanics Reviews* **49**(7), 365–379.
URL: *https://doi.org/10.1115/1.3101931*

Guo, R. W. and Seddon, J. (1983), 'The swirl in an s-duct of typical air intake proportions', *The Aeronautical Quarterly* **34**(2), 99–129.
URL: *https://doi.org/10.1017/S0001925900009641*

Haug, J. P., Rademakers, R. P. M., Stößel, M. and Niehuis, R. (2018), Numerical flow field analysis in a highly bent intake duct, *in* 'Proceedings of ASME Turbo Expo 2018: Power for Land, Sea and Air', ASME GT2018-76633.
URL: *https://doi.org/10.1115/GT2018-76633*

Hawthorne, W. R. (1951), 'Secondary circulation in fluid flow', *Proceedings of the Royal Society of London. Series A. Mathematical and Physical Sciences* **206**(1086), 374–387.
URL: *https://doi.org/10.1098/rspa.1951.0076*

Keerthi, M. C., Kushari, A. and Somasundaram, V. (2017), 'Experimental study of suction flow control effectiveness in a serpentine intake', *Journal of Fluids Engineering* **139**(10).
URL: *https://doi.org/10.1115/1.4036827*

Max, P., Petroll, C. and Niehuis, R. (2020), 'Besondere Herausforderungen für Messrechen zur Untersuchung von stark gekrümmten Triebwerkseinläufen in einer Kleintriebwerksversuchsanlage', *Deutsche Gesellschaft für Luft- und Raumfahrt - Lilienthal-Oberth e.V .*
URL: *https://doi.org/10.25967/530129*

Rabe, A. C. (2003), Effectiveness of a serpentine inlet duct flow control scheme at design and off-design simulated flight conditions, PhD thesis, Virginia Tech.

Rademakers, R. P., Haug, J. P., Niehuis, R. and Stößel, M. (2016), Design and development of a military engine inlet research duct, *in* '30th Congress of the International Council of the Aeronautical Sciences, DCC, Daejeon, Korea'.

Rao, G. A. and Mahulikar, S. P. (2002), 'Integrated review of stealth technology and its role in airpower', *Aeronautical Journal* **106**(1066), 629–642.

Reichert, B. A. and Wendt, B. J. (1996), 'Improving curved subsonic diffuser performance with vortex generators', *AIAA Journal* **34**(1), 65–72.
URL: *https://doi.org/10.2514/3.13022*

Reichert, B. and Wendt, B. (1994), Improving diffusing s-duct performance by secondary flow control, *in* '32nd Aerospace Sciences Meeting and Exhibit', American Institute of Aeronautics and Astronautics, Reston, Virigina.
URL: *https://doi.org/10.2514/6.1994-365*

Reid, C., ed. (1969), *The Response of Axial Flow Compressors to Intake Flow Distortion*, Vol. ASME 1969 Gas Turbine Conference and Products Show of *Turbo Expo: Power for Land, Sea, and Air*.
URL: *https://doi.org/10.1115/69-GT-29*

Squire, H. B. and Winter, K. G. (1951), 'The secondary flow in a cascade of airfoils in a nonuniform stream', *Journal of the Aeronautical Sciences* **18**(4), 271–277.
URL: *https://doi.org/10.2514/8.1925*

Turbine Engine Inlet Flow Distortion Committee, S. (2017), 'Gas turbine engine inlet flow distortion guidelines', *SAE ARP1420C* .
URL: *https://doi.org/10.4271/ARP1420C*

Wong, S. K., Riseborough, E., Duff, G. and Chan, K. K. (2006), 'Radar cross-section measurements of a full-scale aircraft duct/engine structure', *IEEE transactions on antennas and propagation* **54**(8), 2436–2441.
URL: *https://doi.org/10.1109/TAP.2006.879223*